Interaction of Fusidic Acid with Lipid Membranes: Implications to the Mechanism of Antibiotic Activity

Emma Falck,* Jari T. Hautala,† Mikko Karttunen,‡§ Paavo K. J. Kinnunen,¶ Michael Patra,§‖ Heikki Saaren-Seppälä,**†† Ilpo Vattulainen,‡‡§§¶¶ Susanne K. Wiedmer,† and Juha M. Holopainen¶**

*Beckman Institute for Advanced Science and Technology, University of Illinois at Urbana-Champaign, Urbana, Illinois; †Laboratory of Analytical Chemistry, Department of Chemistry, University of Helsinki, Helsinki, Finland; ‡Department of Applied Mathematics, The University of Western Ontario, London, Ontario, Canada; §Biophysics and Statistical Mechanics Group, Laboratory for Computational Engineering, Helsinki University of Technology, Helsinki, Finland; ¶Helsinki Biophysics and Biomembrane Group, Institute of Biomedicine, Biomedicum, University of Helsinki, Helsinki, Finland; ‖Physical Chemistry 1, Lund University, Lund, Sweden; **Department of Ophthalmology, University of Helsinki, Helsinki, Finland; ††Department of Ophthalmology, Itä-Savo Hospital District, Helsinki, Finland; ‡‡Laboratory of Physics and Helsinki Institute of Physics, Helsinki University of Technology, Helsinki, Finland; §§Institute of Physics, Tampere University of Technology, Tampere, Finland, and ¶¶MEMPHYS-Center for Biomembrane Physics, Physics Department, University of Southern Denmark, Odense, Denmark

ABSTRACT We have studied the effects of cholesterol and steroid-based antibiotic fusidic acid (FA) on the behavior of lipid bilayers using a variety of experimental techniques together with atomic-scale molecular dynamics simulations. Capillary electrophoretic measurements showed that FA was incorporated into fluid 1-palmitoyl-2-oleoyl-*sn*-glycero-3-phosphocholine membranes. Differential scanning calorimetry in turn showed that FA only slightly altered the thermodynamic properties of 1,2-dipalmitoyl-*sn*-glycero-3-phosphocholine (DPPC) bilayers, whereas cholesterol abolished all endotherms when the mole fraction of cholesterol (X_{chol}) was >0.20. Fluorescence spectroscopy was then used to further characterize the influence of these two steroids on DPPC large unilamellar vesicles. In the case of FA, our result strongly suggested that FA was organized into lateral microdomains with increased water penetration into the membrane. For cholesterol/DPPC mixtures, fluorescence spectroscopy results were compatible with the formation of the liquid-ordered phase. A comparison of FA and cholesterol-induced effects on DPPC bilayers through atomistic molecular dynamics simulations showed that both FA and cholesterol tend to order neighboring lipid chains. However, the ordering effect of FA was slightly weaker than that of cholesterol, and especially for deprotonated FA the difference was significant. Summarizing, our results show that FA is readily incorporated into the lipid bilayer where it is likely to be enriched into lateral microdomains. These domains could facilitate the association of elongation factor-G into lipid rafts in living bacteria, enhancing markedly the antibiotic efficacy of FA.

INTRODUCTION

Fusidic acid (FA, see Fig. 1) is a hydrophobic, steroid-based, narrow spectrum antibiotic derived from *Fusidium coccineum* and has been used to treat infections with gram-positive *Staphylococcus aureus* (1). Interestingly, it is also effective against corynebacteria, nocardia, anaerobes, and gram-negative *Neisseria* species (2). Fusidic acid inhibits polypeptide chain elongation by binding to the ribosome-elongation factor-G (EF-G)-GDP complex and thereby preventing the dissociation of EF-G from the ribosome (3). FA is effective in prokaryotes because they contain only one elongation factor. Eukaryotes, however, contain several other factors that are not inhibited by FA (2). The crystal structure of EF-G was resolved more than 10 years ago (4,5) and the translocation machinery in *Escherichia coli* has also been visualized using three dimensional cryoelectron microscopy (6). FA binds to EF-G at a stoichiometry of 1:1 (7). Accordingly, for FA to reach intracellular EF-G, it first has to interact with bacterial membranes. Then, it may either randomly diffuse within the bacteria to an EF-G containing location or remain partitioned within the membrane. In the latter case EF-G has to be attached to the outer bacterial membrane where it may interact with FA. Ribosomes are able to interact directly with lipid membranes (8). Accordingly, detailed knowledge of FA-lipid membrane interactions is essential to understand and possibly to enhance the antimicrobial activity of FA and similar agents.

Lipid bilayer is a structure that forms the core of all membranes, and proteins and carbohydrates are embedded into it. Biological membranes are dynamic, adaptive and cooperative supramolecular assemblies. Accordingly, a number of membrane binding and embedded ligands, membrane lipid, protein, and carbohydrate composition, and a number of physical parameters modulate the state of the membrane. Sterols, and particularly cholesterol, (see Fig. 1) may form up to 50% of the total lipid fraction of the membrane. High sterol content implies that they not only regulate certain cellular machineries through direct interaction with proteins, but may also regulate the function of cellular membranes via determining their physical properties (9). Due to their amphiphilic nature, sterols are intercalated in membranes with their hydrophilic group(s) positioned, on the average, at the hydrophobic-hydrophilic interface and with the

Submitted March 8, 2006, and accepted for publication June 6, 2006.

Address reprint requests to Juha Holopainen, Dept. of Ophthalmology, University of Helsinki, PO Box 220, FI-00029 HUS, Helsinki, Finland. Tel.: 358-9-471-77197; Fax: 358-9-471-73162, E-mail: holopainen.juha@gmail.com.

0006-3495/06/09/1787/13 $2.00

doi: 10.1529/biophysj.106.084525

hydrophobic steroid skeleton embedded in the bilayer core. Cholesterol molecules are essentially rigid and relatively smooth in their hydrophobic parts. When incorporated into a lipid bilayer, a cholesterol molecule prefers to have ordered lipid chains surrounding it. Due to their bulkiness, sterols also tend to break interactions between adjacent phospholipid acyl chains (10,11). It has been suggested that at relatively high sterol concentrations, especially cholesterol, a new so-called liquid-ordered phase arises. That phase has a relatively high conformational order and a fairly high lateral diffusion (10–15). It is these new emerging phases, and possibly the formation of lateral heterogeneity in the plane of the membrane, that in part regulate the function of molecular machinery of the cell.

The nongenomic effects of steroids require much higher concentrations to manifest themselves than those mediated by the nuclear steroid receptors (16). Although these nongenomic effects are well documented, their mechanisms are still being disputed. One likely possibility is that these effects are mediated via the membrane lipid matrix (17,18) as suggested for amphotericin B (19), or through changes in the protein-water interface (17). For example, anesthetic efficiencies of steroid-based anesthetics correlate with the partitioning of the drug into the membrane-water interface (20) and with the extent of membrane perturbation caused by these drugs (17,18,21). Furthermore, the cardiotoxicity of doxorubicin (22) and pulmonary toxicity of amiodarone (23) seem to be mediated via the cellular membranes.

Notably, hydrophobicity of compounds is directly linked to their membrane partitioning. The high capacity of FA for tissue penetration (e.g., Hansen (24)) has been ascribed to the surface activity and the lipid solubility of the drug (25), but this has not been adequately studied. Here we have studied the partitioning of FA into lipid bilayers and FA-phospholipid interactions both experimentally (by means of capillary electrochromatography, differential scanning calorimetry, and fluorescence spectroscopy) as well as through molecular dynamics (MD) simulations. We have compared these effects to those exerted by incorporation of cholesterol. We conclude that FA is embedded in the lipid membrane where it causes minor perturbations to the dynamics of the phospholipids. However, it induces lateral microheterogeneity that may be important for its antimicrobial activity. Phospholipid/cholesterol mixtures behave very differently. Incorporation of cholesterol into lipid bilayers gradually shifts the bilayer into a liquid-ordered phase with relatively lower lateral diffusion rates and relatively higher conformational order compared to fluid bilayers, as has been suggested previously (10,12,15).

MATERIALS AND METHODS

Materials

Androstenedione, d-aldosterone, EDTA, FA, HEPES, and 1-palmitoyl-2-oleoyl-*sn*-glycero-3-phosphocholine (POPC) were purchased from Sigma and 1,2-dipalmitoyl-*sn*-glycero-3-phosphocholine (DPPC) from Coatsome (Amagasaki, Hyogo, Japan). 1-Palmitoyl-2[10-(pyren-1-yl)]decanoyl-*sn*-glycero-3-phosphocholine (PyrPC) was from K&V Bioware (Espoo, Finland), and 1,6-dipheny1,3,5-hexatriene (DPH) and Laurdan from Molecular Probes (Eugene, OR). Progesterone was from Merck (Darmstadt, Germany). Methanol was from Mallinckrodt Baker (Deventer, The Netherlands). The purity of the above lipids was checked by thin-layer chromatography on silicic acid-coated plates (Merck) using chloroform/methanol/water (65:25:4, v/v/v) for phospholipids as a solvent system. Examination of the plates after iodine staining revealed no impurities. The purity of fluorescent probes was verified by thin-layer chromatography under ultraviolet (UV)-illumination. Concentrations of the phospholipids were determined gravimetrically using a high precision electrobalance (Cahn, Cerritos, CA), and those of the fluorescent probes by measuring their absorbance at the absorption maximum and using appropriate molar extinction coefficients provided by Molecular Probes and K&V Bioware. Water was freshly deionized in a Milli RO/Milli Q (Millipore, Bedford, MA) filtering system.

Liposome preparation

Appropriate amounts of the lipid stock solutions were mixed in chloroform to obtain the desired compositions. For fluorescence spectroscopy experiments, PyrPC ($X = 0.01$), DPH ($X = 0.002$), or Laurdan ($X = 0.01$) were included as a fluorescent probe. The resulting mixtures were then evaporated to dryness under a stream of nitrogen and traces of solvent removed by evacuating under reduced pressure for 6–24 h. The lipid residues were hydrated at 65°C in 5 mM HEPES, 0.1 mM EDTA (pH = 7.4) buffer to yield multilamellar vesicles with a lipid concentration of 0.7–2 mM, and maintained at this temperature for 30 min. Thereafter the suspensions were irradiated for 2 min in a bath type ultrasonicator (NEY Ultrasonik 104H, Yucaipa, CA). The resulting dispersions were subsequently processed to large unilamellar vesicles (LUVs) by extrusion through a Millipore 0.1 μm pore size polycarbonate filter using a Liposofast low pressure homogenizer (Avestin, Ottawa, Canada).

Capillary electrochromatographic measurements

A Hewlett Packard ^{3D}CE system (Agilent, Waldbronn, Germany) equipped with a diode array detector (detection at 200, 204, and 245 nm) was used for the electrophoretic measurements. Uncoated fused-silica capillaries were from Composite Metal Services (Worcestershire, UK). Dimensions of the used capillaries were 50 μm inner diameter (375 μm outer diameter) with the length of the capillary to the detector 51.5 cm and the total length 60 cm.

The steroid samples for capillary electrochromatographic (CEC) studies were prepared from stock solutions of steroids (1–2 mg ml^{-1} in methanol). The concentrations of analytes in the injected sample were 20 μg ml^{-1} for aldosterone and androstenedione, and 50 μg ml^{-1} for progesterone in 9/191 vol/vol methanol/5 mM HEPES, 0.1 mM EDTA, pH 7.4 solution. Methanol was used as a marker for the electroosmotic flow (EOF). The FA sample contained 2 mM of FA in 5 mM HEPES, 0.1 mM EDTA, at pH 7.4. All solutions were stored in a refrigerator.

Capillary coating

For the studies with POPC/FA coatings, a fresh capillary was rinsed with a pressure of 930–940 mbar for 10 min with 0.5 M nitric acid and for 15 min with water. Coating was applied to the capillary inner surface as follows: after preconditioning, the capillary was rinsed for 10 min with 2 mM liposome solution at 930–940 mbar, after which it was left to stand filled with the liposome solution for 15 min, followed by 5 mM HEPES, 0.1 mM EDTA, pH 7.4 rinse (10 minutes) before first run with each capillary. In addition, the capillary was rinsed for 1 min with liposome solution and for 3

min with 5 mM HEPES, 0.1 mM EDTA, pH 7.4 solution before each run to refresh the coating and to prevent the regeneration of it. New, fresh capillary was employed for each measurement series of different phospholipid coatings. The quality of the coating and the effect of FA on it was studied by measuring the EOF—a change in the surface charge or packing of coating will change the EOF—and the interaction of neutral analytes with the coating.

CEC separation conditions were as follows: voltage 20 kV, temperature of the capillary cassette 25°C, sample injection 5 s at 50 mbar, and detection at 200 nm for methanol, at 204 nm for FA and at 245 nm for steroids. Separations of analytes were repeated six times with each sample. Same coating was used for steroid and FA sample runs. The durability of coating and its properties was ensured by one steroid run, which was compared to previous steroid separations, after FA sample runs. During series of runs, the quality of the 5 mM HEPES, 0.1 mM EDTA, pH 7.4 solution was ensured by use of own buffer vials for each sample (steroid and FA).

Separation of neutral analytes in coated capillaries is based solely on their interaction with the membrane. Thus, factors such as hydrophobicity or lipophilicity of the analyte, and permeability of the membrane, determine the migration order of these components. The retention factor can be used to measure the interaction of an analyte with the coating. The chromatographic retention factor (k'):

$$k' = \frac{t_m - t_{eo}}{t_{eo}}, \quad (1)$$

where migration times of the analyte (t_m) and an unretained component (t_{eo}) is used to describe the ratio of the time that the analyte stays in the stationary phase versus the time that the analyte is carried by the mobile phase. However, Eq. 1 holds only for uncharged analytes and we have also used anionic FA in our study. Thus, more sophisticated calculations are needed.

The retention factor in CEC has been studied by many groups recently (26–28). Rathore and Horváth (27) introduced the k'' as a measure of chromatographic retention under conditions of the CEC experiments. k'' measures the magnitude of the retention due to the reversible binding of analytes to the CEC stationary phase and holds for both uncharged and charged analytes:

$$k'' = \frac{t_m(1 + k''_e) - t_{eo}}{t_{eo}}, \quad (2)$$

where k''_e is the velocity factor $k''_e = t_{ep}/t_{eo}$ (t_{ep} is the electrophoretic mobility of analyte in uncoated capillary and t_{eo} is the electroosmotic mobility in the coated capillary). Wiedmer et al. (28) transformed Eq. 2, for cases of phospholipid coated capillaries and interaction studies, into a more convenient form:

$$k'' = t_m\left(\frac{1}{t_{eo}} + \frac{1}{t_{m'}} + \frac{1}{t_{eo'}}\right) - 1, \quad (3)$$

where t_m' and t_{eo}' are respectively migration times of analyte and electroosmotic flow in the uncoated capillary. Equation 3 was used to measure the retention of analytes also in this study. Capillary electrophoresis was employed to determine the migration times of analytes (t_m') and EOF (t_{eo}') in uncoated capillary.

Differential scanning calorimetry

Differential heat capacity scans were recorded at a lipid concentration of 0.7 mM (multilamellar vesicles) and at a heating rate of 0.5°C/min. Before their loading into precooled differential scanning calorimetry (DSC) cuvettes, the samples were equilibrated on ice for ~24 h and were thereafter degassed at low pressure. The calorimeter (VP-DSC, MicroCal, Northampton, MA) was interfaced to a PC and data were analyzed using the routines of the software provided with the instrument. All samples were scanned by heating from 10°C to 80°C. All experiments were done in duplicates.

Measurement of I_e/I_m for PyrPC

A monomeric excited state pyrene may relax to its ground state by emitting photons with a maximum wavelength at ~380 nm (I_m), the exact peak energy and spectral fine structure depending on solvent polarity. During its lifetime, the excited state pyrene may also form a characteristic short-lived complex, excimer (excited dimer), with a ground-state pyrene. This complex relaxes back to two ground-state pyrenes by emitting quanta as a broad and featureless band centered at ~480 nm (I_e). Essentially, the excimer/monomer fluorescence intensity ratio (I_e/I_m) is proportional to the rate of collisions between the pyrenes. For a single pyrene moiety containing lipid analog such as PyrPC, the value for I_e/I_m reflects the lateral mobility as well as the local concentration of the fluorophore in the membrane (29). Fluorescence emission spectra for LUVs labeled with PyrPC were recorded with a PerkinElmer (Wellesley, MA) LS50B spectrofluorometer equipped with a magnetically stirred, thermostated cuvette compartment. Excitation wavelength was 344 nm and the excitation and emission bandwidths were 4 nm; 2 ml of liposome solution (50 nmoles of lipid) in a four-window quartz cuvette were used in each measurement. Each sample was equilibrated for 2 min before recording of spectrum. Three scans were averaged and the emission intensities at ~380 and 480 nm were taken for I_m and I_e, respectively. As only relative values were of interest, the measured spectra were not corrected for instrument response. All experiments were done in triplicates.

Fluorescence anisotropy of DPH

Anisotropy depends on the average angular motion of the fluorophore (30). Increase in membrane free volume V_f allows for more extensive wobbling of the fluorophore, and thus decreases fluorescence anisotropy r (31). Conversely, increase in this parameter proposes increased membrane order and reduction in V_f. Steady-state r for DPH has been shown to be proportional to its lifetime (e.g., 31,32), and Parasassi et al. (33) pointed out that changes in DPH lifetime and chain order in membranes to be compensatory. Recent atomistic simulations are also in favor of using free DPH for studies of membrane order close to the probe (34,35). Nevertheless, care needed in the interpretation of DPH measurements since the fluorescence anisotropy of DPH provides only indirect information of membrane ordering in the vicinity of the probe. That is in contrast to 2H NMR, which yields explicit information about the order of lipid acyl chains.

DPH was included into liposomes to yield a lipid/DPH molar ratio of 500:1. Polarized emission was measured in the L-format using polaroid film type prisms in the PerkinElmer LS50B spectrofluorometer. Excitation at 360 nm and emission at 450 nm were selected with monochromators and using 5 nm bandwidths. The samples were maintained in the cuvette for 2 min before the measurement of anisotropy, averaging the signal over a 15 s interval. Values of steady-state fluorescence anisotropy r were calculated using routines of the software provided by PerkinElmer and data analyzed using Microsoft Excel. All experiments were performed three times.

Fluorescence generalized polarization for Laurdan

The polarity- and hydration-sensitive probe Laurdan resides in the interfacial region of the membrane (36). Laurdan was included into vesicles at mole fraction $X_{lipid}/X_{Laurdan} = 100{:}1$. Generalized polarization (GP) of Laurdan reports on changes in the microenvironment of the probe, and GP value is mainly sensitive to hydration and water dynamics within the interface (36). One important determinant of interfacial hydration is the distance between lipid backbones. For a series of similar lipids (e.g., zwitterionic or anionic) the Laurdan GP value decreases linearly with increasing interbackbone distance (37). Both excitation and emission bandpasses for the measurement

were set at 5 nm. Excitation was at 350 nm, and GP was calculated from the emission intensities at 440 nm (I_{440}) and 480 nm (I_{480}) by

$$GP = (I_{440} - I_{480})/(I_{440} + I_{480}).$$

Experiments were repeated three times.

Atomistic molecular dynamics simulations

Initial configurations for atomic-scale molecular dynamics simulations including DPPC and FA molecules were based on our previous studies of DPPC bilayers, consisting of 64 DPPC molecules per leaflet (38). These fully equilibrated structures were complemented by extra water to increase the number of water molecules from 28 to 38 per lipid. The simulated systems are fully hydrated, or essentially under similar conditions. Structures of DPPC and FA molecules are shown in Fig. 1. Since we consider both the protonated (neutral FA) and the deprotonated case (charged FA), there are two descriptions for fusidic acid.

Nine DPPC molecules were replaced by FA in each leaflet of the bilayer resulting in a molar concentration of 14%. Each individual fusidic acid molecule replacing one DPPC was set in a membrane such that its orientation was in line with the orientation of the removed DPPC molecule.

The above gives us two sets of initial coordinates, one for the COOH case (protonated COO-group, neutral fusidic acid) and another for the COO case (deprotonated COO-group, charged fusidic acid). In the below discussion, these two cases are denoted by COOH and COO, in respective order. For COO, sodium counter ions are added (39) to account for electroneutrality.

Simulations followed a standard procedure described elsewhere (38). For fusidic acid, no force field is available to the authors' knowledge, and hence a new force field based on the GROMOS/GROMACS force fields was developed (available from http://www.softsimu.org/downloads.shtml). For consistency, the effect of the Lennard-Jones potential beyond the cutoff was approximated on a mean-field level, resulting in an almost constant offset to the pressure. This, together with smaller hydration levels in earlier simulations leads to small differences compared with previous simulations (38,39). For this reason, a reference simulation of a pure DPPC bilayer was also conducted.

After energy minimization, the system was preequilibrated by simulating for 100 ps with a time step of 1 fs in the absence of constraints. Subsequently, the main simulations were started at $t = 0$ and continued for 100 ns. The temperature was set to $T = 50$°C to be in the physiologically relevant phase above the main phase transition temperature of ~41°C. The simulations had equilibrated after 20 ns, allowing us to use the remaining 80 ns of each trajectory for data analysis.

To facilitate the comparison of FA- and cholesterol-induced effects, we also analyze and discuss our previous simulation data (40,41) for a bilayer mixture of DPPC and cholesterol at $X_{chol} = 0.13$ at $T = 50$°C.

RESULTS

Incorporation of fusidic acid into phospholipids bilayers studied by capillary electrochromatography

CEC with silica capillaries coated with unilamellar phospholipid has been shown to be a powerful tool for analyzing the characteristics of phospholipid membranes and for studying phospholipids-analyte interactions (28,42–44). Therefore, CEC was used in this study to determine the possible interaction between FA and POPC bilayers. For the case of experimental simplicity, POPC instead of DPPC was used in these experiments—at room temperature POPC is fluid whereas DPPC is in the gel phase. Capillaries were coated using different liposome solutions (2 mM POPC/FA (mole fraction of FA (X_{FA}) = 0, 0.20, and 0.40) in 5 mM HEPES, 0.1 mM EDTA, pH 7.4) as a coating material. Electroosmotic flows (EOF) with different coatings as well as the interaction of these coatings with steroids and FA were measured to show possible changes in membrane characteristics due to the presence of FA.

The EOF in capillaries with different coatings is shown in Fig. 2, and it can be seen that the EOF increases linearly ($R^2 = 0.9981$) as a function of FA in the coating. The net charge of POPC at pH 7.4 is close to zero, whereas FA is negatively charged (the pK_a value of FA is 4.1 ± 0.4). When the capillary is coated with POPC, the EOF clearly decreases compared to an uncoated one (~6.058×10^{-4} cm^2/Vs). Adding FA to the bilayers increases its negative surface charge/net charge, which also increases the EOF in the capillary. Thus it can be concluded that FA remains in the membrane after coating with POPC/FA liposomes.

Studies on how FA as a sample interacts with different coatings were also carried out (Fig. 3). The interaction of FA with the coating clearly decreased as the amount of FA in the coating increased. Thus, FA interacts more strongly with pure POPC coatings than with coatings containing FA. The basic structure of FA (common for steroids) is hydrophobic, but there are also hydrophilic groups attached. Because of this, the hydrophilicity and net charge of the coatings

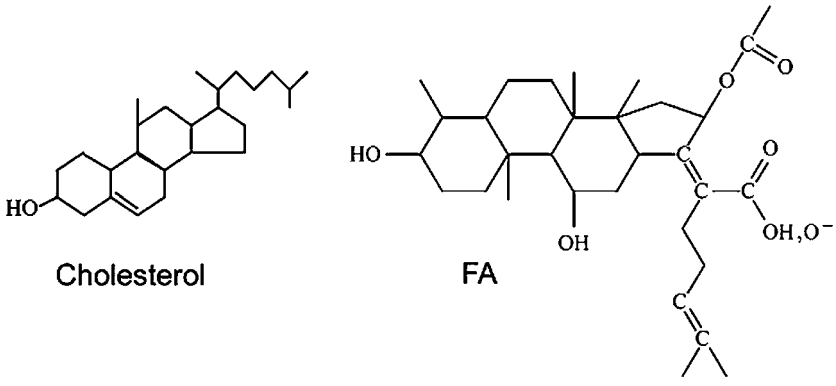

FIGURE 1 Structures of cholesterol and fusidic acid molecules studied in this work. For fusidic acid, we consider two cases: the neutral molecule (−COOH) and the charged one (−COO).

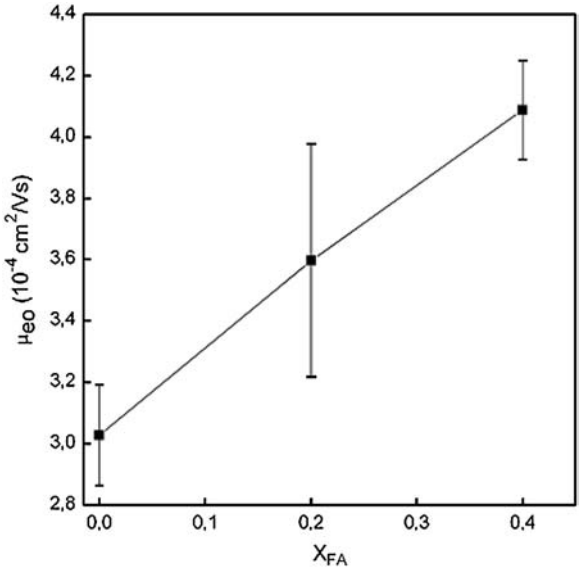

FIGURE 2 EOF in capillaries with different coatings. Error bars represent standard deviation multiplied by 2. Running conditions: fused-silica capillary, total length 60 cm; length to detector 51.5 cm; inner diameter 50 μm, outer diameter 375 μm; capillary temperature 25°C; sample injection 5 s at 50 mbar; applied voltage 20 kV; and UV detection 200 nm.

increase with increasing amounts of FA in the membrane. The retention of FA (as a sample) decreases as well.

The decrease in the permeability of the membrane as a function of increasing amounts of FA can also be seen with the steroid sample (aldosterone, androstenedione, and progesterone) (Fig. 4). Of the three steroids used, progesterone is the most hydrophobic one. The interaction between the steroids and the coating starts to decrease when the amount of FA in the membrane increases. The difference in the retention of steroids in POPC- and POPC/FA 80:20-coated capillaries is rather small, but with the POPC/FA 60:40 coating, a clear decrease in retention (k'') is observed.

Our CE results indicate that FA is within the phospholipid membrane. In addition, the changes in EOF and retention of FA were quite linear (three-point calibration). Thus, when FA-containing liposomes were used for coating capillaries, FA remained in the coating (membrane).

Effects of fusidic acid and cholesterol on the thermotropic behavior of DPPC multilamellar vesicles

Representative DSC upscans for pure DPPC and mixed DPPC/FA and DPPC/cholesterol are illustrated in Fig. 5, panels *A* and *B*, respectively. Neat DPPC showed three transitions: a subtransition at $T_s = 16.8 \pm 0.20$°C, a pretransition at $T_p = 34.9 \pm 0.06$°C, and a main transition at $T_m = 41.3 \pm 0.03$°C. These results are in agreement with previously published data (45). The enthalpy of the main phase transition peak for DPPC was 8.57 ± 0.12 kcal/mol and the peak width of this transition was 0.17 ± 0.01°C.

The sub- and pretransition disappeared already at $X_{FA} = 0.10$ in two out of three DSC runs; in one run, a transition

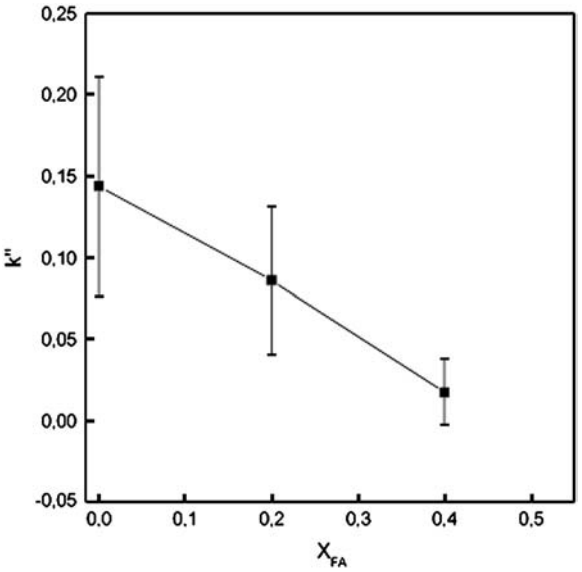

FIGURE 3 Retention factor of FA in capillaries with different POPC/FA coatings. Error bars represent standard deviation multiplied by 2. Running conditions: fused-silica capillary, total length 60 cm; length to detector 51.5 cm; inner diameter 50 μm, outer diameter 375 μm; capillary temperature 25°C; sample injection 5 s at 50 mbar; applied voltage 20 kV; and UV detection 204 nm.

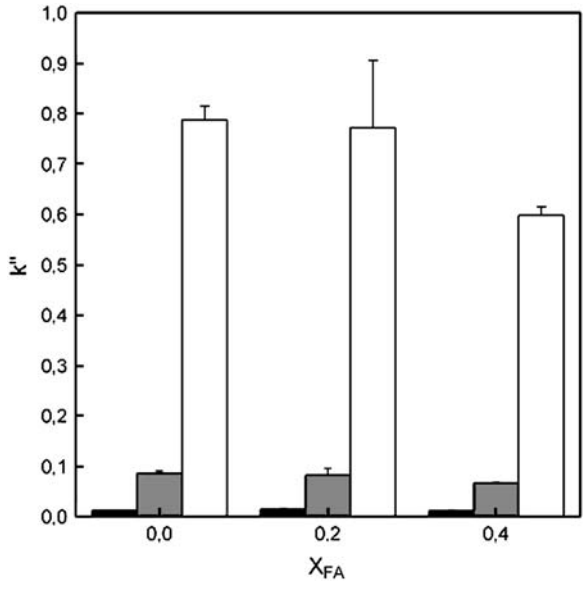

FIGURE 4 Retention factors of the steroids aldosterone (*solid*), androstenedione (*shaded*), and progesterone (*open*) in capillaries with different POPC/FA coatings. Error bars represent standard deviation multiplied by 2. Running conditions: fused-silica capillary, total length 60 cm; length to detector 51.5 cm; inner diameter 50 μm, outer diameter 375 μm; capillary temperature 25°C; sample injection 5 s at 50 mbar; applied voltage 20 kV; and UV detection 200 and 245 nm.

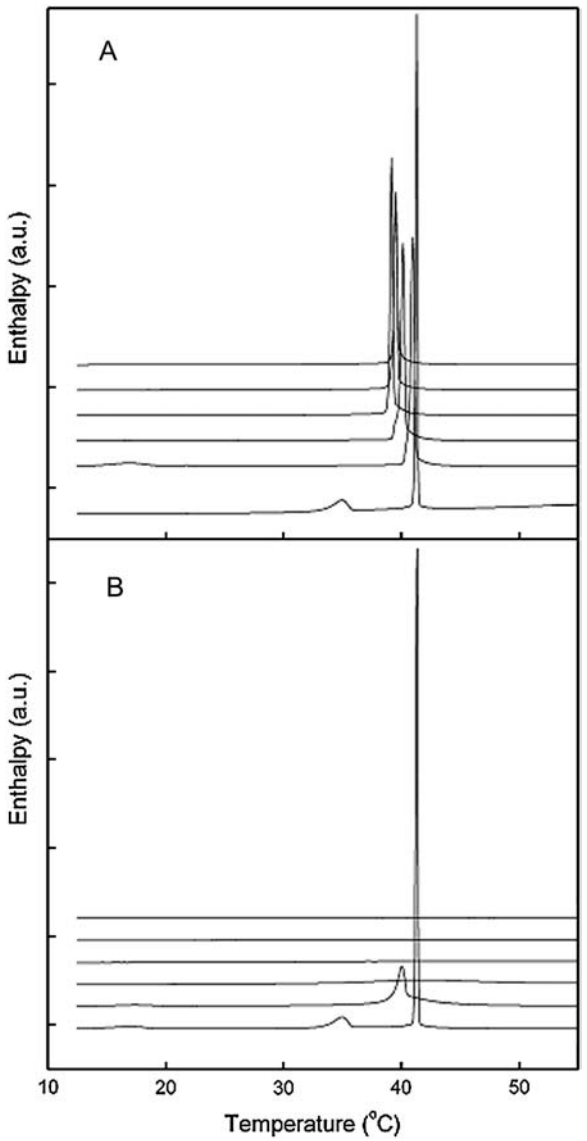

FIGURE 5 High-sensitivity differential-scanning calorimetry heating scans for multilamellar DPPC/fusidic acid (*A*) and DPPC/cholesterol (*B*) vesicles. The mole fractions of sterol were 0, 0.1, 0.20, 0.30, 0.40, and 0.50 from bottom to top. The total lipid concentration was 0.7mM in 5mM HEPES, 0.1mM EDTA (pH 7.4).

was observed at 17.0°C, as shown in Fig. 5 *A*. Further increase in FA abolished all transitions except the main phase transition with no new peaks emerging at the thermograms. However, the main phase transition peak became asymmetric with a shoulder evident at the low temperature side. This shoulder became the main endotherm at increasing X_{FA}. Accordingly, increasing X_{FA} from 0 to 0.5 decreased the main phase transition temperature (T_m) of DPPC gradually from 41.3 to 40.1°C, broadened the T_m from 0.17 to 0.34°C, and decreased main phase transition enthalpy (ΔH) of DPPC from 8.6 to 4.8 kcal/mol. These results implicate that the cooperativity of the bilayers is decreased and possibly suggest formation of lateral microheterogeneity.

Incorporating cholesterol at $X_{chol} = 0.10$ decreased T_m from 41.3 to 40.0°C, suppressed the pretransition, decreased the enthalpy of the main transition, and simultaneously the peak width of the main phase transition widened (Fig. 5 *B*). Further increase of cholesterol concentration up to $X_{chol} = 0.20$–0.30 made it difficult to identify the endotherm due to their low cooperativity characterized by a significantly increased peak width and reduced ΔH. For $X_{chol} > 0.30$, the thermograms did not show any discernible phase transitions.

Characterization of DPPC/fusidic acid and DPPC/cholesterol bilayers by fluorescence spectroscopy

Pyrene

For fluorescent probes such as PyrPC containing a single pyrene moiety, I_e/I_m depends on the rate of intermolecular collisions between pyrene moieties. Accordingly, this parameter can be used to observe phase separation and changes in the dynamics of bilayers (29,46). At 30°C, DPPC bilayers are in the gel (solid-ordered) state and PyrPC is highly enriched into microdomains indicated by the high I_e/I_m ratio. Increasing the content of FA up to $X_{FA} = 0.50$ caused a gradual increase in the I_e/I_m ratio for PyrPC (Fig. 6). At $T = 50$°C, when DPPC bilayers are in the fluid (liquid crystalline) state, no segregation of PyrPC is observed. Increasing the content of FA up to $X_{FA} = 0.50$ caused a gradual increase in the I_e/I_m ratio for PyrPC similarly to the gel bilayers. These results suggest either that FA induces lateral microheterogeneity or enhances lateral diffusion. For

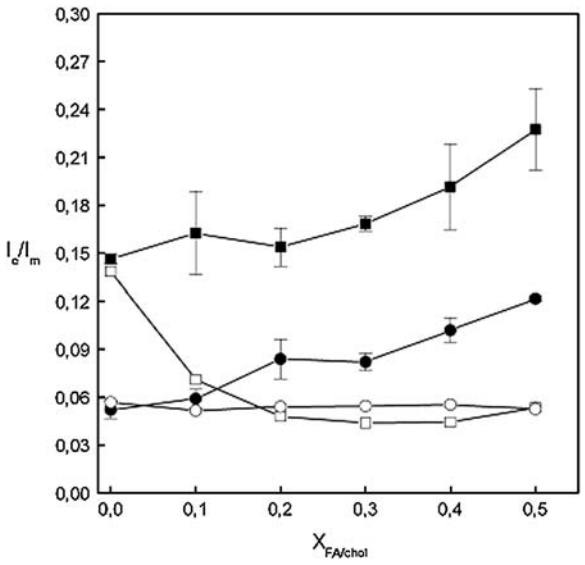

FIGURE 6 Intermolecular I_e/I_m for PyrPC ($X = 0.01$) measured for LUVs composed of DPPC and the indicated contents of fusidic acid (*solid symbols*) or cholesterol (*open symbols*). The total lipid concentration was 22.5 μM in 5 mM HEPES, 0.1 mM EDTA, pH 7.4. The temperature was maintained at 30 (□) and 50 (○) °C with a circulating water bath.

cholesterol, however, the behavior is very different. At 30°C, increasing the cholesterol content from $X_{chol} = 0$ to 0.20 decreased the I_e/I_m ratio for PyrPC from 0.14 to 0.05, whereafter a further increase in X_{chol} had no effect (Fig. 6). In the fluid state, increasing the content of cholesterol from $X_{chol} = 0$ to 0.50 had no apparent effect on the I_e/I_m ratio for PyrPC. Thus, in the gel state, cholesterol reduces lateral diffusion or solubilizes PyrPC from the formed microdomains. In the fluid state, cholesterol seems not to have an apparent impact on the behavior of PyrPC (Fig. 6). Other experiments such as fluorescence recovery after photobleaching and NMR indicate, though, that in the fluid phase, cholesterol reduces lateral diffusion (15,47).

DPH

To gain further insight into the organization of DPPC-steroid bilayers, we measured anisotropy (r) for DPH as a function of X_{sterol}. Below T_m, the acyl chains are highly ordered, the free volume is low, and the wobbling motion of DPH is highly hindered. As a result, r is high (48). When $T < T_m$, increasing X_{FA} from 0 to 0.1 increased r from 0.32 to 0.36, suggesting increased acyl chain order. For exceeding $X_{FA} = 0.1$, no further changes in r were observed (Fig. 7). In the fluid state, however, a modest decrease in r is observed upon incorporating increasing amounts of FA. That indicates that DPH may possibly wobble more extensively in the presence of FA (Fig. 7).

The system behaves very differently in the presence of cholesterol. When $T < T_m$, including cholesterol into DPPC bilayers up to a mole fraction of 0.20 causes a decrease in r from 0.32 to 0.27, whereafter no apparent changes are observed (Fig. 7). For $T > T_m$ (DPPC), the opposite behavior is observed: increasing X_{chol} from 0 to 0.5 increases r more than twofold (Fig. 7). This is in line with the proposal that cholesterol increases the acyl chain order and decreases lateral diffusion, as expected (10,12,15).

Laurdan

Laurdan is sparingly soluble in water, and accordingly the generalized polarization (GP) value reflects the relaxation of water molecules adjacent to the fluorescent probe in phospholipid membranes. Thus, this fluorophore can be used to monitor water penetration into the bilayers. The higher the GP value, the lower is the penetration of water (33,36,49). At both below and above T_m, a small decrease in GP is observed upon incorporating FA up to $X_{FA} = 0.50$, indicating increased water penetration into the membranes (Fig. 8). For $T < T_m$ (DPPC), cholesterol (up to $X_{chol} = 0.50$) induces a negligible effect on Laurdan GP. When $T > T_m$, however, incorporating cholesterol up to $X_{chol} = 0.30$ increases GP for Laurdan fourfold, indicating that cholesterol prevents penetration of water into the bilayers (Fig. 8). Further increase in X_{chol} did not have any impact on GP.

FA and cholesterol induced ordering of lipid acyl chains studied through atomic-scale molecular dynamics simulations

The above experiments raise a number of intriguing questions regarding the influence of FA on membrane

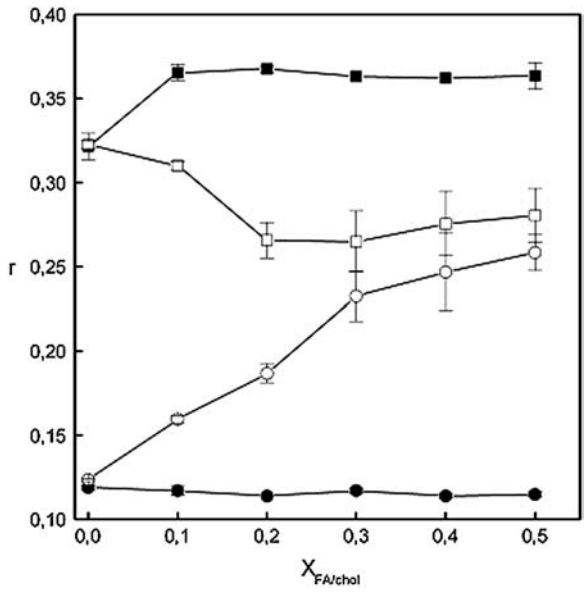

FIGURE 7 Fluorescence anisotropy r for DPH ($X = 0.002$) residing in binary LUVs composed of DPPC and fusidic acid (*solid symbols*) or cholesterol (*open symbols*). The temperature was maintained at 30 (□) and 50 (○) °C with a circulating water bath. Otherwise conditions were as described in the legend for Fig. 2.

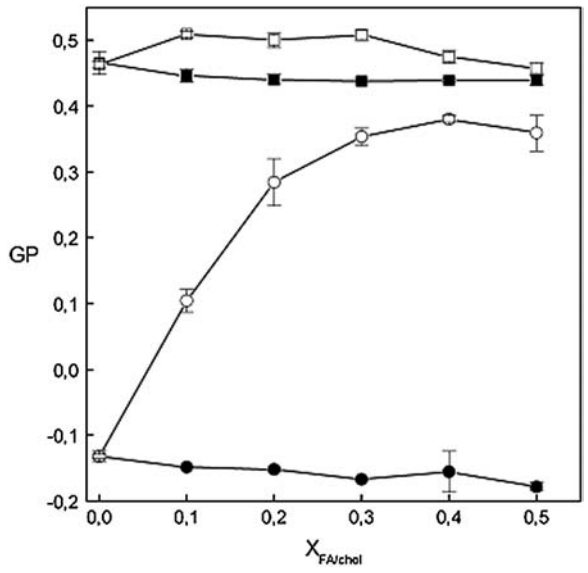

FIGURE 8 Effect of increasing sterol/phosphatidylcholine ratio on the GP of Laurdan in DPPC liposomes at 30 (□) and 50°C (○). The solid and open symbols represent data for fusidic acid and cholesterol, respectively. The data points represent averages of three measurements, and error bars represent standard deviation. The lipid concentration was 25 μM in 5 mM HEPES and 0.1 mM EDTA, pH 7.4.

properties. In the following, we consider some of them through atomistic simulations comparing FA-induced effects to those of cholesterol.

Fig. 9 shows the NMR order parameter profiles ($|S_{CD}|$ averaged over the sn-1 and sn-2 chains of DPPC) for DPPC/FA ($X_{FA} = 0.14$) and DPPC/cholesterol ($X_{chol} = 0.13$) systems. For details of the order parameter calculation, see Falck et al. (40). We find that the ordering effect of the neutral FA (−COOH) is almost identical to that of cholesterol, the ordering effect of FA being slightly weaker. The ordering capability of the charged FA (−COO), however, is significantly weaker than that of cholesterol, and the difference is particularly clear in the middle of the acyl chain region and close to the tails. Studies of the average area per molecule ($\langle A \rangle$) support these findings. For DPPC/cholesterol, we found $\langle A \rangle = 0.54$ nm^2, for DPPC/FA with neutral FA $\langle A \rangle = 0.55$ nm^2, and for DPPC/FA with charged FA molecules $\langle A \rangle = 0.58$ nm^2. These trends are consistent with the somewhat general observation that for sterols, the smaller the area per molecule, the larger is the lipid acyl chain ordering.

We can conclude that DPPC/FA systems remain fluid-like. The ordered nature of DPPC/FA systems is less pronounced compared to DPPC/cholesterol systems, however. We return to this issue below where we discuss the density profiles of the membranes.

Lateral diffusion in DPPC/FA and DPPC/cholesterol bilayers

To characterize the lateral diffusion of individual DPPC molecules in the bilayer plane, we computed the lateral diffusion coefficient D of DPPCs in DPPC/FA and DPPC/cholesterol mixtures through MD simulations (see Falck et al. (40,50)) for details of calculations). Since the simulation timescale and statistics limit this procedure, we only consider the diffusion at short times (and calculate the mean-squared displacement for times between 5 and 10 ns) where the error estimates with respect to actual results are reasonable. Hence, the below values should be considered as suggestive.

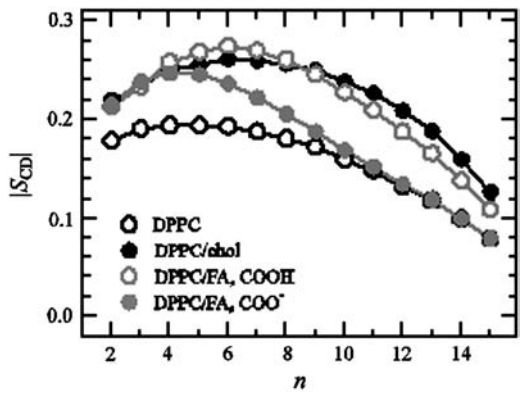

FIGURE 9 NMR order parameter profiles ($|S_{CD}|$) for DPPC. Results are shown for the neat DPPC bilayer, for the DPPC/cholesterol system at $X_{chol} =$ 13 mol %, and for the DPPC/FA system at 14 mol %. In the case of FA, results for two cases are depicted: the neutral FA (−COOH) and the charged FA (−COO). The results shown in each case are averages over the sn-1 and sn-2 chains since their behavior was almost identical. Small carbon numbers correspond to CH2 groups close to the glycerol group in DPPC, and large carbon numbers correspond to the end of the chain (see Fig. 1).

In the fluid phase above the main phase transition temperature, we found $D = 10 \pm 2 \times 10^{-8}$ cm^2/s in the pure DPPC system. This is consistent with NMR spectroscopic and fluorescence recovery after photobleaching experiments, which have found D values between ~6 and 15×10^{-8} cm^2/s (see Falck et al. (40,50)) and references therein). In the mixtures, we found $D = 1.6 \pm 0.3 \times 10^{-8}$ cm^2/s in DPPC/FA (COOH) and $D = 1.2 \pm 0.3 \times 10^{-8}$ cm^2/s in DPPC/FA (COO) systems. For comparison, in the DPPC/cholesterol bilayer, the diffusion coefficient was found to be $3.8 \pm 0.8 \times 10^{-8}$ cm^2/s. This indicates that the lateral diffusion in systems containing FA is reduced compared to DPPC/cholesterol mixtures (also see below). Evidently, bearing in mind the above experimental results for PyrPC and DPH, this supports the view that FA is likely to be enriched into lateral microdomains.

Distribution of FA, cholesterol, and free volume in a membrane

We analyzed the mass density profiles of FA and cholesterol in a bilayer and compared their orientational distributions. Mass density profiles in Fig. 10, *a* and *b*, show that the two FA systems behave somewhat differently. Although in both cases the FA molecules are located roughly in the middle of the hydrophobic acyl chain region, the location of the COOH (COO) group is different. In the case of neutral FA, the COOH group has a bimodal shape with two peaks at 0.55 and 1.2 nm from membrane center, whereas in the charged case, the COO group is closer to the water phase, having a broad peak ~1.4 nm from the center of the membrane. Results in Fig. 10 *c* for DPPC/cholesterol indicate that the density profile of cholesterol resembles the neutral COOH case of FA more closely than the profile of the charged FA.

A closer inspection reveals that the differences in density profiles and acyl chain ordering are due to differences in the orientational distribution of FA (COOH and COO) and cholesterol. The cholesterol stands almost in an upright position along the membrane normal. As for FA, although the COOH case stands roughly in a similar manner, the COO case is considerably different as its charged COO group lies close to the membrane-water interface. This distinctly different behavior is characterized by the average tilt of the molecules with respect to membrane normal: we describe the principal axis of cholesterol and FA molecules by a vector starting at the carbon connected to the tail and ending at the carbon connected to the hydroxyl group (see Fig. 1). For cholesterol, the average tilt angle of this vector with respect to membrane normal is 23.5°. For the COOH case of FA, it is 66.4, and for the COO case, ~105°. The strongly tilted

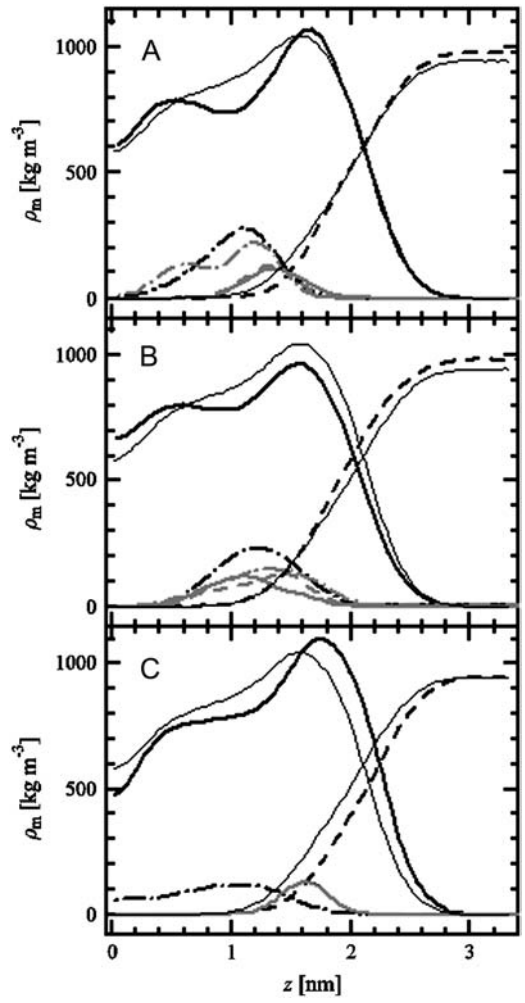

FIGURE 10 Mass density profiles through the bilayer as a function of the distance from membrane center (z). (*a*) FA/DPPC system (COOH), (*b*) FA/DPPC mixture (COO), and (*c*) DPPC/cholesterol bilayer. A detailed description of each panel is as follows. (Panels *a* and *b*) Lipids (*solid black*), water (*dashed black*), FA (*dash-dotted black*), hydroxyl-chol (*solid shaded*), hydroxyl-FA (*dashed shaded*), and carboxyl-group (*dash-dotted shaded*). (Panel *c*) Lipids (*solid black*), water (*dashed black*), cholesterol (*dash-dotted black*), and hydroxyl-chol (*solid shaded*). Above, hydroxyl-chol stands for the hydroxyl group associated with cholesterol (attached to carbon 3 in cholesterol, and also included in FA), whereas hydroxyl-FA refers to the OH-group attached to the third ring in FA. Results for the mass densities of hydroxyl and carboxyl groups have been scaled by a factor of 10 to clarify the presentation. For comparison, the profiles of lipids and water in a neat DPPC system are also given in every panel (*thin solid lines*).

orientation of FA (COO) disturbs the packing and ordering of nearby lipids (see Fig. 9 for NMR order parameter profiles) and leads to increased free volume in the middle of the bilayer. This is characterized by a striking difference in the interdigitation of FA and cholesterol molecules: whereas ~35% of cholesterols interdigitate to the opposing leaflet, FAs do not interdigitate at all. In fact, we find little or no FA in the center of the bilayer. A thorough analysis of free volume distribution, void sizes, and shapes (see Falck and collaborators (40,41,51)) for a description of the analysis) supports these conclusions. A more detailed account of these issues will be given elsewhere.

Summarizing, FA, and in particular the charged FA, leads to significant perturbations in a membrane, creating additional free volume pockets and increasing the free volume especially close to the membrane center in the hydrophobic region of the membrane. This provides a reasonable explanation for the above DPH results, proposing that the location of DPH in a DPPC/FA membrane is different from the neat DPPC or DPPC/cholesterol cases. Unlike cholesterol, FA is strongly tilted with respect to the bilayer normal, which implies that the average cross-sectional area of FA in the bilayer plane is larger than that of cholesterol. The motion of DPPCs surrounded by FAs is then more constrained compared to the DPPC/cholesterol case, which likely explains why the lateral diffusion in FA containing membranes is slower than in the DPPC/cholesterol system.

DISCUSSION

The capillary electrochromatographic, as well as DSC and fluorescence spectroscopy measurements, clearly indicate that FA is incorporated into fluid phospholipid bilayers, as expected from its molecular structure. DSC is particularly useful in characterizing the thermodynamic behavior of lipid bilayers and accordingly it has been used to investigate phase boundaries in different lipid mixtures (e.g., Mabrey and Sturtevant (52) and Holopainen et al. (53)). However, this technique does not provide any structural information. With increasing sterol concentrations, a broadening of the pure lipid gel-to-fluid phase transition into a gel-fluid two-phase coexistence region was observed for both sterols. The effect is much more pronounced for cholesterol. From previous studies and the one presented here, we can conclude that incorporating cholesterol at $X_{cho} \sim 0.25$–0.30 induces the formation of the liquid-ordered phase. For FA this is less evident. The likely reason for this is that due to its less-smooth surface and attached hydrophilic tails, FA does not possess an equally prominent ordering effect on the acyl chains of DPPC. Comparison of cholesterol and lanosterol, lanosterol being less smooth than cholesterol, leads to a similar conclusion: the ordering effect of lanosterol is considerably weaker than that of cholesterol, and consequently the coexistence regime for liquid-disordered and liquid-ordered phases at intermediate lanosterol concentrations seems to disappear (11). Recent experiments and simulations in which desmosterol and cholesterol were compared for their ability to promote lipid rafts also support the above view (54). The present MD simulations suggest that the structural smoothness of sterol-like molecules plays a role: they show that the ordering of DPPC chains in the presence of FA is weaker than in the presence of an equal amount of cholesterol. In particular, the charged FA perturbs the membrane significantly, leading to only a relatively weak ordering of lipid acyl chains.

For FA below T_m, the I_e/I_m ratio for PyrPC is initially high because of lateral segregation of the probe (55). That is due to hydrophobic mismatch between the highly ordered acyl chains of DPPC and the less-ordered and bulky fluorescent probe (56,57). Incorporating FA into the membranes further increased this ratio. This might be due to an increase in lateral diffusion or the possibility that FA still enhances the segregation of PyrPC into microdomains. The anisotropy for DPH was increased below T_m. Based on this, one may expect that either the acyl chain order is increased or the lateral diffusion is diminished, or both. Furthermore, a small decrease in GP for Laurdan is observed under the influence of FA, suggesting that water molecules are more easily penetrating into the bilayer, possibly due to formation of domain boundaries.

Above T_m, the I_e/I_m ratio for PyrPC in DPPC bilayers was low, indicating that PyrPC was evenly dispersed into the membrane (55). Increasing X_{FA} in DPPC bilayers enhanced significantly the I_e/I_m ratio for PyrPC. Above T_m, a slight decrease in r for DPH is observed, which may implicate slightly increased lateral diffusion or more likely a small disordering effect around the probe. The magnitude of this effect was, however, negligible. It thus seems evident that also above T_m, increasing the content of FA forced the probe into lateral microdomains. Simultaneously, upon increasing X_{FA} decreased GP for Laurdan. This finding indicates an increase in water penetration and may reflect the formation of domain boundaries, increased lateral diffusion, or increased lipid backbone distance (37). From these, increased lateral diffusion was ruled out by our MD simulation results.

The minor impact of FA on the acyl chain order of DPPC was proposed by DPH anisotropy. This is in line with MD simulations showing that lipid acyl chains in charged FA (COO) containing membranes were significantly less ordered compared to membranes including an equal amount of cholesterol. This finding suggests, furthermore, that FA residing in lipid bilayers is in the charged state as suggested by its low pK_a value.

Further, it was perhaps surprising to find that Laurdan GP values were only slightly affected by the presence of FA at both 30°C and 50°C. This result is in contrast to our previous findings using pregnanolone, a water insoluble anesthetic, which demonstrated that this steroid resided at the interfacial region of the lipid bilayers (58). It should be kept in mind that the chemical structure of pregnanolone is simpler and resembles more closely cholesterol than FA does. This may indicate that the orientation of pregnanolone in phosphatidylcholine bilayers resembles that of cholesterol. Paclitaxel, a drug used for the treatment of several types of cancer, is highly lipophilic and has some structural similarities to FA. As is observed for FA, paclitaxel lowers T_m, broadens the main phase transition peak, and reduces ΔH for DPPC bilayers (59). Likewise, anesthetic steroid alphaxalone and nonsteroidal antiestrogen Tamoxifen show similar effects on DPPC bilayers as FA (60,61). In the latter case also, changes in DPH anisotropy and Laurdan GP were measured. These results showed that practically there was no change in either parameter (61) and thus parallel closely the results of this study. The effect of the decrease in T_m was explained by the ''excluded volume interaction'' theory (62). In keeping with this theory, any substance that decreases molecular interactions and packing properties of the acyl chains will lead to a broader main phase transition endotherm which peaks at lower temperatures. It was suggested that Tamoxifen was located at the upper 10 carbons of the acyl chains (61). Experimental results presented here cannot pledge the location of FA, but MD simulations show that FA resides roughly in the middle of the hydrophobic acyl chain region, the peak of the mass density profile of FA being ~1.15 nm from membrane center.

Taken together, DSC, fluorescence spectroscopy, and simulation results suggest that FA induces formation of lateral microdomains. The support based on simulations is indirect, though, since the domain formation takes place over times much larger than those simulated here.

A similar reasoning can be applied to DPPC/cholesterol mixtures. Below T_m, cholesterol induced a large decrement in the I_e/I_m ratio for PyrPC, indicating either that the microdomains were dispersed leading to diminished excimer formation for pyrene or that lateral diffusion was increased. This may be due to the thinning effect that cholesterol causes on DPPC bilayers for $T < T_m$ and accordingly the hydrophobic mismatch between the probe and acyl chains of DPPC diminishes (57). Anisotropy for DPH decreases upon increasing X_{chol}, probably leading to a decrease in the acyl chain order (and thinning of the membrane) and increment in lateral diffusion. No significant changes in GP for Laurdan were observed, demonstrating that water penetration into the lipid bilayer was not changed. This finding seems strange: we would expect that increment in lateral diffusion would also render the bilayer to be more hydrated. This lack of effect for $T < T_m$ (DPPC) was also seen for DPPC/FA mixtures, and thus suggests that although significant changes are induced into the hydrocarbon region of the bilayer by incorporation of sterols, the changes do not affect the interfacial region of the membrane.

Above T_m, for DPPC the I_e/I_m ratio for PyrPC was unaltered upon increasing X_{chol} from 0 to 0.5. It has been suggested that cholesterol forms some type of lipid microdomains (11,63–65) with coexistence of pure PC and PC-cholesterol domains. However, the sizes of these domains are expected to be very small (of the order of tens of nanometers, see Loura et al. (66)) and their lifetime is short. Accordingly, these domains are inaccessible by experiments. This might explain why we do not observe an increase in the I_e/I_m ratio for PyrPC upon increasing X_{chol}. The lateral diffusion decreased and acyl chain order increased upon addition of cholesterol into DPPC bilayers indicated by MD simulations and supported by an increase in DPH anisotropy.

Simultaneously, GP for Laurdan increased substantially, showing that water penetration into the bilayer diminished. The likely reason for the increase in GP in cholesterol containing membranes is that cholesterol displaces water from the interface and decreases the number of water molecules within the immediate vicinity of Laurdan. Feigenson and collaborators have suggested that due to the very small headgroup of cholesterol, the adjacent phospholipids have to form an ''umbrella'' to cover the steroid molecule to avoid water penetration into the bilayers interior (63,67). Simultaneously, the bilayer becomes more condensed (68). This is reflected also as an increase in DPH anisotropy (Fig. 7).

The GP value for Laurdan reaches maximum at about $X_{chol} \sim 0.30$ (50°C) after which no apparent changes are observed. Likewise for DPH anisotropy, the largest change in this parameter is seen at $X_{chol} \leq 0.30$. This is in agreement with the formation of the liquid-ordered phase (10,12,13,15) and with those reports showing that for $X_{chol} \geq 0.30$, the lipid diffusion coefficient does not vary much (15,48,69). The liquid-ordered phase is characterized by a rapid axially symmetric motion and fast lateral diffusion, which is comparable, albeit lower, than in fluid bilayers (12). Yet the orientational order and spectral moments are significantly higher than those in fluid phospholipid bilayers (12). Further proof of nearly homogenous phase derives from measurements of I_e/I_m for PyrPC showing that at 50°C, no changes in this parameter are observed.

FA is likely to be enriched into lateral microdomains or ''lipid rafts'' (70). These could significantly increase the availability of FA to interact with its target protein, EG-F. Accordingly, we consider it unlikely that FA would freely diffuse within the interior of the bacteria and finally reach its target protein. Such a mechanism would also be very inefficient; for such system to be feasible, very high concentrations of FA would be needed. Obviously, that is not the case. Instead, our results show that FA resides in the membrane and is enriched into lateral microdomains leading to high local concentrations. These platforms could dock also EG-F and ribosomes within the same lateral area of the membrane. This type of mechanism would enhance the inhibition of polypeptide elongation by several orders of magnitude (71). Finally, the results presented in our study necessitate a more thorough investigation of the mechanism of drug-induced lateral domain formation to enhance more efficient antimicrobial activity.

The Mary and Georg C. Ehrnrooth Foundation (J.M.H.), Sigrid Juselius Foundation (J.M.H.), Oskar Huttunen Foundation (J.M.H.), Academy of Finland (E.F., I.V., M.K., P.K.J.K., J.T.H., and S.K.W.), and Emil Aaltonen Foundation (M.K.) supported this study.

REFERENCES

1. Verbist, L. 1990. The antimicrobial activity of fusidic acid. *Antimicrob. Chemother.* 25(Suppl. B):1–5.
2. Collignon, P., and J. Turridge. 1999. Fusidic acid in vitro activity. *Int. J. Antimicrob. Agents.* 12(Suppl. 2):S45–S58.
3. Tanaka, N., T. Kinoshita, and H. Masukawa. 1968. Mechanism of protein synthesis inhibition by fusidic acid and related antibiotics. *Biochem. Biophys. Res. Commun.* 30:278–283.
4. Czworkowski, J., J. Wang, T. A. Steitz, and P. B. Moore. 1994. The crystal structure of elongation factor G complexed with GDP, at 2.7 Å resolution. *EMBO J.* 13:3661–3668.
5. Ævarsson, A., E. Brazhnikov, M. Garber, J. Zheltonosova, Y. Chirgadze, S. al-Karadaghi, L. A. Svensson, and A. Liljas. 1994. Three-dimensional structure of the ribosomal translocase: elongation factor G from *Thermus thermophilus*. *EMBO J.* 13:3669–3677.
6. Agrawal, R. K., P. Penczek, R. A. Grassucci, and J. Frank. 1998. Visualization of elongation factor G on the *Escherichia coli* 70S ribosome: the mechanism of translocation. *Proc. Natl. Acad. Sci. USA.* 95:6134–6138.
7. Willie, G. R., N. Richman, W. P. Godtfredsen, and J. W. Bodley. 1975. Some characteristics of and structural requirements for the interaction of 24,25-dihydrofusidic acid with ribosome—elongation factor G complexes. *Biochemistry.* 14:1713–1718.
8. Savitz, A. J., and D. I. Meyer. 1997. Receptor-mediated ribosome binding to liposomes depends on lipid composition. *J. Biol. Chem.* 272: 13140–13145.
9. Mouritsen, O. G., and M. J. Zuckermann. 2004. What's so special about cholesterol? *Lipids.* 39:1101–1113.
10. Ipsen, J. H., G. Karlström, O. G. Mouritsen, H. Wennerström, and M. J. Zuckermann. 1987. Phase equilibria in the phosphatidylcholine-cholesterol system. *Biochim. Biophys. Acta.* 905:162–172.
11. Miao, L., M. Nielsen, J. Thewalt, J. H. Ipsen, M. Bloom, M. J. Zuckermann, and O. G. Mouritsen. 2002. From lanosterol to cholesterol: structural evolution and differential effects on lipid bilayers. *Biophys. J.* 82:1429–1444.
12. Vist, M. R., and J. H. Davis. 1990. Phase equilibria of cholesterol/dipalmitoylphosphatidylcholine mixtures: 2H nuclear magnetic resonance and differential scanning calorimetry. *Biochemistry.* 29:451–464.
13. Sankaram, M. B., and T. E. Thompson. 1990. Interaction of cholesterol with various glycerophospholipids and sphingomyelin. *Biochemistry.* 29:10670–10675.
14. Sankaram, M. B., and T. E. Thompson. 1990. Modulation of phospholipid acyl chain order by cholesterol. A solid-state 2H nuclear magnetic resonance study. *Biochemistry.* 29:10676–10684.
15. Almeida, P. F., W. L. Vaz, and T. E. Thompson. 1992. Lateral diffusion in the liquid phases of dimyristoylphosphatidylcholine/cholesterol lipid bilayers: a free volume analysis. *Biochemistry.* 31: 6739–6747.
16. Duval, D., S. Durant, and F. Homo-Delarche. 1983. Non-genomic effects of steroids. Interactions of steroid molecules with membrane structures and functions. *Biochim. Biophys. Acta.* 737:409–422.
17. Makriyannis, A., D. P. Yang, and T. Mavromoustakos. 1990. The molecular features of membrane perturbation by anesthetic steroids: a study using differential scanning calorimetry, small angle X-ray diffraction and solid state ^{2}H NMR. *Ciba Found. Symp.* 153:172–189.
18. Ueda, I., T. Tatara, J. S. Chiou, P. R. Krishna, and H. Kamaya. 1994. Structure-selective anesthetic action of steroids: anesthetic potency and effects on lipid and protein. *Anesth. Analg.* 78:718–725.
19. Bolard, J. 1986. How do the polyene macrolide antibiotic affect the cellular membrane properties? *Biochim. Biophys. Acta.* 864:297–304.
20. Ueda, I., and T. Yoshida. 1999. Hydration of lipid membranes and action mechanisms of anesthetics and alcohols. *Chem. Phys. Lipids.* 101:65–79.
21. Makriyannis, A., C. M. DiMeglio, and S. W. Fesik. 1991. Anesthetic steroid mobility in model membrane preparations as examined by high-resolution ^{1}H and ^{2}H NMR spectroscopy. *J. Med. Chem.* 34:1700–1703.
22. Goormaghtigh, E., R. Brasseur, and J. M. Ruysschaert. 1982. Adriamycin inactivates cytochrome *c* oxidase by exclusion of the

enzyme from its cardiolipin essential environment. *Biochem. Biophys. Res. Commun.* 104:314–320.

23. Reasor, M. J., and S. Kacew. 1996. An evaluation of possible mechanisms underlying amiodarone-induced pulmonary toxicity. *Proc. Soc. Exp. Biol. Med.* 212:297–304.
24. Hansen, S. 1985. Intraocular penetration of fusidic acid with topical fucithalmic. *Eur. J. Drug Metab. Pharmacokinet.* 10:329–331.
25. Stewart, G. T. 1964. Steroid antibiotics. *Pharmacotherapie.* 2:137–148.
26. Rathore, A. S., and C. Horváth. 1996. Separation parameters via virtual migration distances in high-performance liquid chromatography, capillary zone electrophoresis and electrokinetic chromatography. *J. Chromatogr. A.* 743:231–246.
27. Rathore, A. S., and C. Horváth. 2002. Chromatographic and electrophoretic migration parameters in capillary electrochromatography. *Electrophoresis.* 23:1211–1216.
28. Wiedmer, S. K., M. Jussila, R. M. S. Hakala, K.-H. Pystynen, and M.-L. Riekkola. 2005. Piperazine-based buffers for liposome coating of capillaries for electrophoresis. *Electrophoresis.* 26:1920–1927.
29. Kinnunen, P. K. J., A. Koiv, and P. Mustonen. 1993. Pyrene-labelled lipids as fluorescent probes in studies on biomembranes and membrane models. *In* Fluorescence Spectroscopy. O. S. Wolfbeis, editor. Springer-Verlag, Berlin. 159–169.
30. Lakowicz, J. R. 1999. Principles of Fluorescence Spectroscopy. Plenum Press, London.
31. Chong, P. L.-G., A. R. Cossins, and G. Weber. 1983. A differential polarized phase fluorometric study of the effects of high hydrostatic pressure upon the fluidity of cellular membranes. *Biochemistry.* 22:409–415.
32. Chong, P. L.-G., and G. Weber. 1983. Pressure dependence of 1,6-diphenyl-1,3,5-hexatriene fluorescence in single-component phosphatidylcholine liposomes. *Biochemistry.* 22:5544–5550.
33. Parasassi, T., G. De Stasio, R. M. Rusch, and E. Gratton. 1991. A photophysical model for diphenylhexatriene fluorescence decay in solvents and in phospholipid vesicles. *Biophys. J.* 59:466–475.
34. Repakova, J., P. Capkova, J. Holopainen, and I. Vattulainen. 2004. Distribution, orientation, and dynamics of DPH probes in DPPC bilayer. *J. Phys. Chem. B.* 108:13438–13448.
35. Repakova, J., J. M. Holopainen, M. R. Morrow, M. C. McDonald, P. Capkova, and I. Vattulainen. 2005. Influence of DPH on the structure and dynamics of a DPPC bilayer. *Biophys. J.* 88:3398–3410.
36. Parasassi, T., E. K. Krasnowska, L. Bagatolli, and E. Gratton. 1998. Laurdan and Prodan as polarity-sensitive fluorescent membrane probes. *J. Fluoresc.* 8:365–373.
37. Bagatolli, L., E. Gratton, and G. D. Fidelio. 1998. Water dynamics in glycosphingolipid aggregates studied by LAURDAN fluorescence. *Biophys. J.* 75:331–341.
38. Patra, M., M. Karttunen, M. T. Hyvönen, E. Falck, and I. Vattulainen. 2003. Molecular dynamics simulations of lipid bilayers: Major artifacts due to truncating electrostatic interactions. *Biophys. J.* 84:3636–3645.
39. Anezo, C., A. H. de Vries, H.-D. Höltje, D. P. Tieleman, and S. J. Marrink. 2003. Methodological issues in lipid bilayer simulations. *J. Phys. Chem. B.* 107:9424–9433.
39. Patra, M., and M. Karttunen. 2004. Systematic comparison of force fields for microscopic simulations of NaCl in aqueous solutions: diffusion, free energy of hydration and structural properties. *J. Comput. Chem.* 25:678–689.
40. Falck, E., M. Patra, M. Karttunen, M. Hyvönen, and I. Vattulainen. 2004. Lessons of slicing membranes: interplay of packing, free area, and lateral diffusion in phospholipid/cholesterol bilayers. *Biophys. J.* 87:1076–1091.
41. Falck, E., M. Patra, M. Karttunen, M. Hyvönen, and I. Vattulainen. 2004. Impact of cholesterol on voids in phospholipid membranes. *J. Chem. Phys.* 121:12676–12689.
42. Hautala, J. T., S. K. Wiedmer, and M.-L. Riekkola. 2004. Anionic liposomes in capillary electrophoresis: effect of calcium on 1-palmitoyl-2-oleyl-*sn*-glycero-3-phosphatidylcholine/phosphatidylserine-coating in silica capillaries. *Anal. Bioanal. Chem.* 378:1769–1776.
43. Hautala, J. T., S. K. Wiedmer, and M.-L. Riekkola. 2005. Influence of pH on formation and stability of phosphatidylcholine/phosphatidylserine coatings in fused-silica capillaries. *Electrophoresis.* 26:176–186.
44. Wiedmer, S. K., M.-L. Riekkola, and M. S. Jussila. 2004. Phospholipids and liposomes in liquid chromatographic and capillary electromigration techniques. *TrAC.* 23:562–582.
45. Silvius, J. R. 1982. Thermotropic phase transitions of pure lipids in model membranes and their modifications by membrane proteins. *In* Lipid-Protein Interactions, Vol. 2. P. C. Jost and O. H. Griffith, editors. Wiley, New York. 239–281.
46. Duportail, G., and P. Lianos. 1996. Fluorescence probing of vesicles using pyrene and pyrene derivatives. *In* Vesicles. M. Rosoff, editor. Marcel Dekker, New York. 295–372.
47. Filippov, A., G. Orädd, and G. Lindblom. 2003. The effect of cholesterol on the lateral diffusion of phospholipids in oriented bilayers. *Biophys. J.* 84:3079–3086.
48. Jähnig, F. 1979. Structural order of lipids and proteins in membranes: evaluation of fluorescence anisotropy data. *Proc. Natl. Acad. Sci. USA.* 76:6361–6365.
49. Parasassi, T., M. Di Stefano, M. Loiero, G. Ravagnan, and E. Gratton. 1994. Cholesterol modifies water concentration and dynamics in phospholipid bilayers: a fluorescence study using Laurdan probe. *Biophys. J.* 66:763–768.
50. Falck, E., M. Patra, M. Karttunen, M. Hyvönen, and I. Vattulainen. 2005. Response to the comment by Almeida et al.: free area theories for lipid bilayers—predictive or not? *Biophys. J.* 89:745–752.
51. Kupiainen, M., E. Falck, S. Ollila, P. Niemelä, A. A. Gurtovenko, M. T. Hyvönen, M. Patra, M. Karttunen, and I. Vattulainen. 2005. Free volume properties of sphingomyelin, DMPC, DPPC, and PLPC bilayers. *J. Computat. Theor. Nanoscience.* 2:401–413.
52. Mabrey, S., and J. M. Sturtevant. 1976. Investigation of phase transitions of lipids and lipid mixtures by sensitivity differential scanning calorimetry. *Proc. Natl. Acad. Sci. USA.* 73:3862–3866.
53. Holopainen, J. M., J. Lemmich, F. Richter, O. G. Mouritsen, G. Rapp, and P. K. Kinnunen. 2000. Dimyristoylphosphatidylcholine/C16:0-ceramide binary liposomes studied by differential scanning calorimetry and wide- and small-angle x-ray scattering. *Biophys. J.* 78:2459–2469.
54. Vainio, S., M. Jansen, M. Koivusalo, T. Róg, M. Karttunen, I. Vattulainen, and E. Ikonen. 2006. Desmosterol cannot replace cholesterol in lipid rafts. *J. Biol. Chem.* 281:348–355.
55. Somerharju, P. J., J. A. Virtanen, K. K. Eklund, P. Vainio, and P. K. Kinnunen. 1985. 1-Palmitoyl-2-pyrenedecanoyl glycerophospholipids as membrane probes: evidence for regular distribution in liquid-crystalline phosphatidylcholine bilayers. *Biochemistry.* 24:2773–2781.
56. Mouritsen, O. G., and M. Bloom. 1984. Mattress model of lipid-protein interactions in membranes. *Biophys. J.* 46:141–153.
57. Lehtonen, J. Y., J. M. Holopainen, and P. K. Kinnunen. 1996. Evidence for the formation of microdomains in liquid crystalline large unilamellar vesicles caused by hydrophobic mismatch of the constituent phospholipids. *Biophys. J.* 70:1753–1760.
58. Alakoskela, J. M., T. Söderlund, J. M. Holopainen, and P. K. Kinnunen. 2004. Dipole potential and head-group spacing are determinants for the membrane partitioning of pregnanolone. *Mol. Pharmacol.* 66:161–168.
59. Ali, S., S. Minchey, A. Janoff, and E. A. Mayhew. 2000. differential scanning calorimetry study of phosphocholines mixed with paclitaxel and its bromoacylated taxanes. *Biophys. J.* 78:246–256.
60. Mavromoustakos, T., D. P. Yang, and A. Makriyannis. 1995. Effects of the anesthetic steroid alphaxalone and its inactive delta 16-analog on the thermotropic properties of membrane bilayers. A model for membrane perturbation. *Biochim. Biophys. Acta.* 1239:257–264.
61. Engelke, M., P. Bojarski, R. Bloß, and H. Diehl. 2001. Tamoxifen perturbs lipid bilayer order and permeability: comparison of DSC, fluorescence anisotropy, Laurdan generalized polarization and carboxyfluorescein leakage studies. *Biophys. Chem.* 90:157–173.

62. Nagle, J. F. 1976. Theory of lipid monolayer and bilayer phase transitions: effect of headgroup interactions. *J. Membr. Biol.* 27:233–250.

63. Huang, J., and G. W. Feigenson. 1999. A microscopic interaction model of maximum solubility of cholesterol in lipid bilayers. *Biophys. J.* 76:2142–2157.

64. Rog, T., and M. Pasenkiewicz-Gierula. 2001. Cholesterol effects on the phosphatidylcholine bilayer nonpolar region: a molecular simulation study. *Biophys. J.* 81:2190–2202.

65. Murtola, T., E. Falck, M. Patra, M. Karttunen, and I. Vattulainen. 2004. Coarse grained model for phospholipid/cholesterol bilayer. *J. Chem. Phys.* 121:9156–9165.

66. Loura, L. M. S., A. Fedorov, and M. Prieto. 2001. Fluid-fluid membrane microheterogeneity: a fluorescence resonance energy transfer study. *Biophys. J.* 80:776–788.

67. Huang, J. 2002. Exploration of molecular interactions in cholesterol superlattices: effect of multibody interactions. *Biophys. J.* 83:1014–1025.

68. Smaby, J. M., M. Momsen, V. S. Kulkarni, and R. E. Brown. 1996. Cholesterol-induced interfacial area condensations of galactosylceramides and sphingomyelins with identical acyl chains. *Biochemistry.* 35:5696–5704.

69. Polson, J., I. Vattulainen, H. Zhu, and M. J. Zuckermann. 2001. Simulation study of lateral diffusion in lipid-sterol bilayer mixtures. *Eur. Phys. J. E.* 5:485–497.

70. Simons, K., and E. Ikonen. 1997. Functional rafts in cell membranes. *Nature.* 387:569–572.

71. Verheij, H. M., A. J. Slotboom, and G. H. de Haas. 1981. Structure and function of phospholipase A2. *Rev. Physiol. Biochem. Pharmacol.* 91:91–203.